Supplementary Information

Efficient Removal of Pb (II) from Water by Magnetic Fe$_3$S$_4$/reduced Graphene Oxide Composites

Long Kong, Zhichun Li, Xueqiong Huang, Shouqiang Huang, Hua Sun, Min Liu, and Liang Li*

School of Environmental Science and Engineering, Shanghai Jiao Tong University, 800 Dongchuan Road, Shanghai 200240, P. R. China
E-mail: liangli117@sjtu.edu.cn; Tel: +86 21 54747567

Supplementary information contains 12 pages, 11 figures, and 4 tables.

Adsorption model:

All the adsorption kinetics data were fitted with two different kinetic models, pseudo-first-order model and pseudo-second- order model, expressed as follows: [1]

$$\ln(q_e - q_t) = lnq_e - k_1 t \qquad (1)$$

$$\frac{t}{q_t} = \frac{1}{k_2 q_e^2} + \frac{1}{q_e} t \qquad (2)$$

Where q_t and q_e are the amount of adsorption at any time t (min) and equilibrium (mg g^{-1}). k_1 (min^{-1}) and k_2(g (mg·min)$^{-1}$) denote the rate constant of pseudo-first-order and pseudo-second-order sorption, respectively.

The Langmuir and Freundlich isotherm model were employed to simulate the adsorption isotherm data and can be described as: [2]

$$\frac{C_e}{q_e} = \frac{C_e}{q_m} + \frac{1}{q_m K_L} \qquad (3)$$

$$lnq_e = lnK_F + \frac{1}{n} lnC_e \qquad (4)$$

where C_e is the equilibrium concentration in the liquid phases (mg L^{-1}), q_m represent the maximum adsorption capacity (mg g^{-1}), respectively. K_L and K_F are Langmuir sorption constant related to the affinity parameter of adsorbent and Freundlich adsorption capacity, respectively. 1/n refers to the Freundlich adsorption intensity parameter.
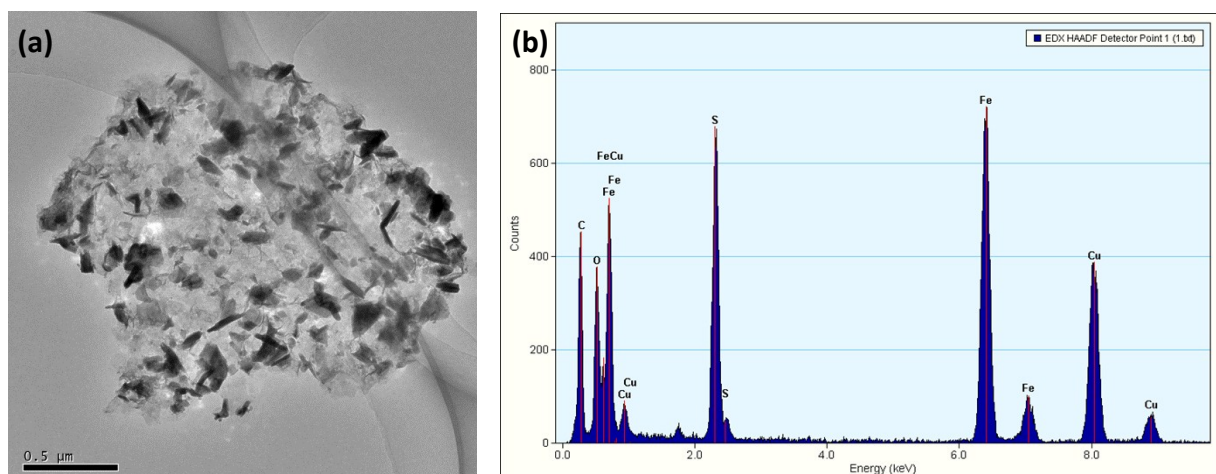
The distribution ratio (K_d) was obtained from the following equation: [3]

$$K_d = \frac{(C_0 - C_e)V}{C_0 \quad m} \qquad (5)$$

Where C_0 is the initial concentration of Pb(II) (mg/L), V denotes the volume of the solution (mL), m is the weight of adsorbent (g).
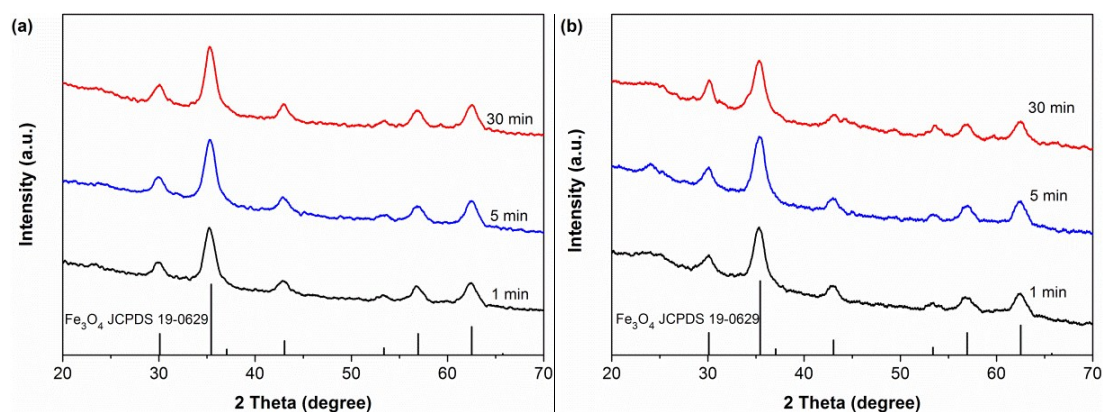
Fig S1 XRD patterns of Fe_3O_4/rGO after the sulfuration reaction using (a) oleylamine and (b) 1-butylamine as solvent for sulfur powders.


Fig S2 (a) TEM images of Fe_3S_4/rGO after the sulfuration over 5 min, (b) EDX results of selected areas of Fe_3S_4/rGO.
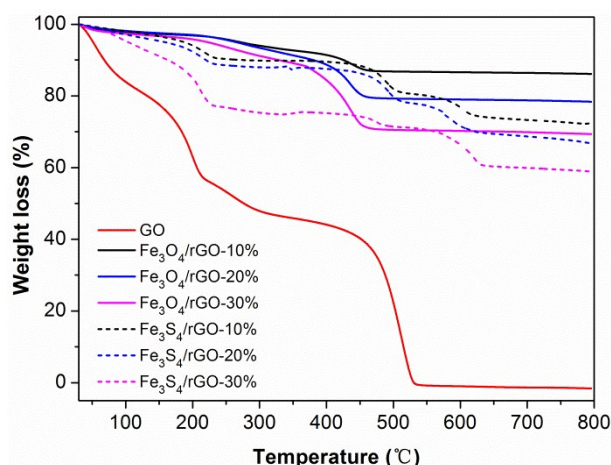
**Fig S3** TGA curves of GO, Fe_3O_4/rGO, and Fe_3S_4/rGO measured from 25 to 800 °C in air atmosphere.

The content of Fe_3O_4 and Fe_3S_4 in the resultant Fe_3O_4/rGO or Fe_3S_4/rGO composites was confirmed by TGA analysis. As shown in Fig S3, the residual weight of Fe_3O_4/rGO was 86.13%, 78.38%, and 69.35% for Fe_3O_4/rGO-10%, Fe_3O_4/rGO-20%, and Fe_3O_4/rGO-30% after the samples was heated to 800 in air.[4] It was pointed out that the Fe_3O_4 phase in the Fe_3O_4/rGO can be oxidized by air to Fe_2O_3. Based on the weight of Fe_2O_3 after 800 °C, the Fe_3O_4 content in Fe_3O_4/rGO-10%, Fe_3O_4/rGO-20%, and Fe_3O_4/rGO-30% was calculated to be 83.25%, 75.77%, and 67.21%. Accordingly, the content of rGO was about 16.75 wt%, 24.23 wt%, and 32.79 wt%, respectively. As for Fe_3S_4/rGO, it exhibited a different thermal oxidative degradation features since Fe_3O_4 and Fe_3S_4 coexisted in the composites. Under test conditions (25-800 °C, air flow), the weight loss of Fe_3S_4/rGO corresponds to the oxidation of Fe_3O_4 and Fe_3S_4 and the decomposition of rGO, leaving the final products as Fe_2O_3. The remaining weight of Fe_3S_4/rGO-10%, Fe_3S_4/rGO-20%, and Fe_3S_4/rGO-30% composites was 72.21%, 66.77%, and 58.89%, respectively. The difference of residual weight between Fe_3O_4/rGO and its corresponding Fe_3S_4/rGO composite was assigned to the weight loss in oxidation process of Fe_3S_4. Therefore, the Fe_3S_4 content was calculated to be about 61.89%, 51.99%, and 47.59% in Fe_3S_4/rGO-10%, Fe_3S_4/rGO-20%, and Fe_3S_4/rGO-30%. The accurate contents of Fe_3O_4 and Fe_3S_4 in the composites were listed in Table S2.
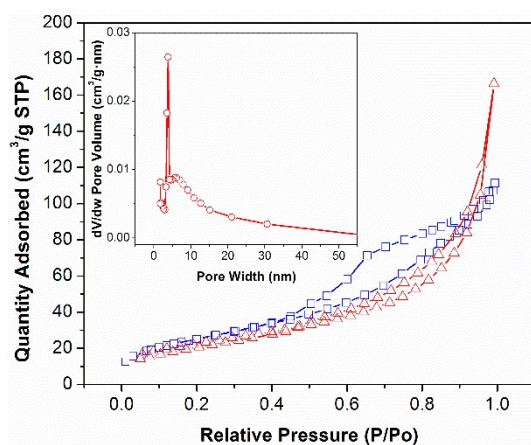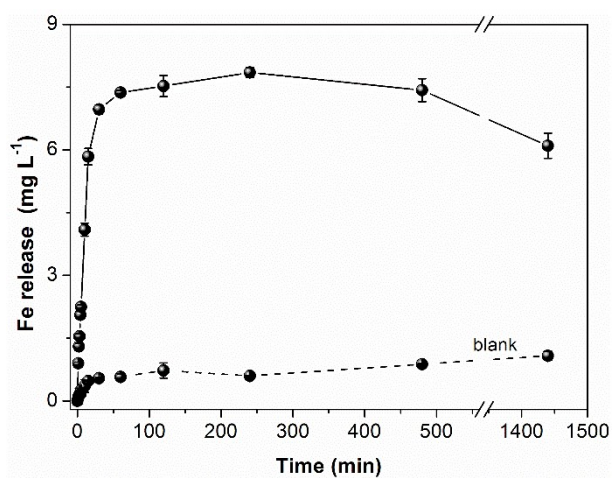
Fig S4 Nitrogen adsorption-desorption isotherms of Fe_3O_4/rGO and Fe_3S_4/rGO. Inset: BJH pore size distribution (mainly 3-4 nm) of Fe_3S_4/rGO.
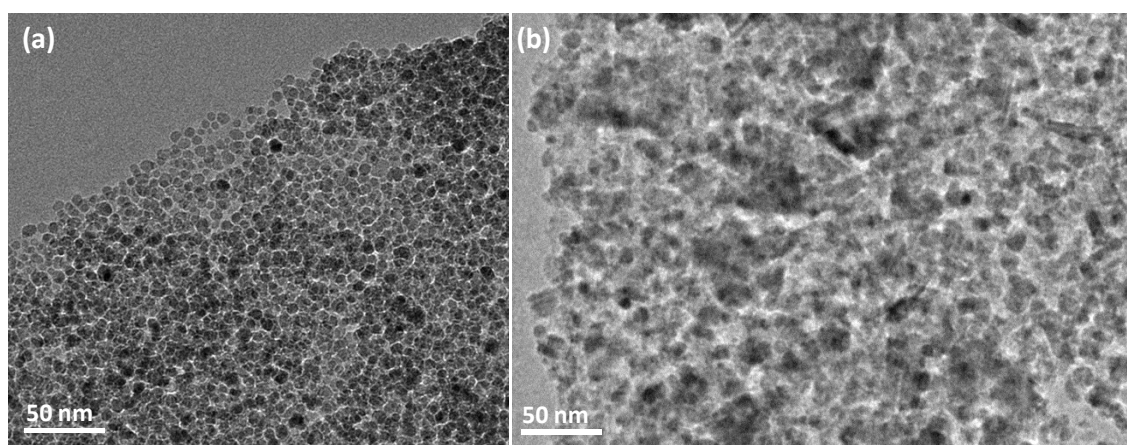
**Fig S5** TEM images of (a) Fe_3O_4/rGO-10% and (b) Fe_3S_4/rGO-10%.
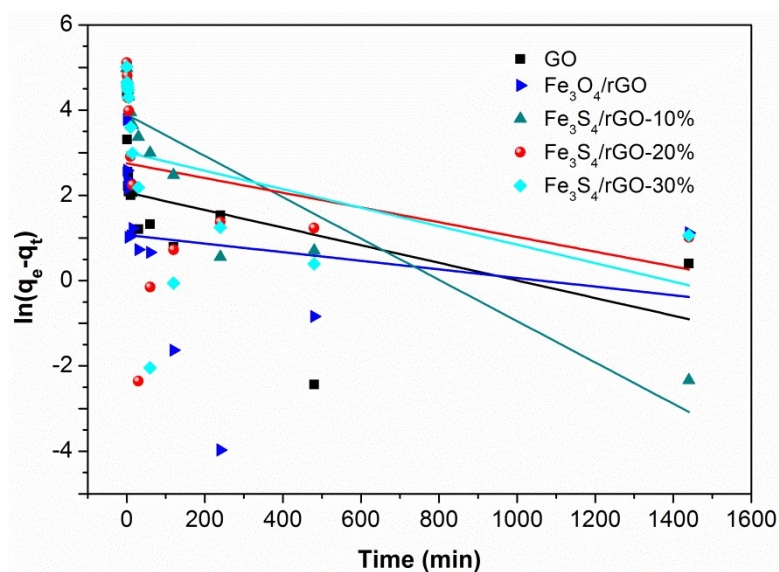
Fig S6 Test of pseudo-first-order model for adsorption of Pb (II) on different adsorbents. The symbols are experimental data and the solid lines represent the fitted curves.

Fig S7 Fe release kinetics of Fe_3S_4/rGO in the adsorption process toward Pb (II). Experimental conditions: initial Pb (II) concentration 50 mg L^{-1} 100 mL, sorbent 25 mg, pH 6, temperature 25 °C. The dash line represented the bank samples, Fe_3S_4/rGO solution without the addition of Pb (II).
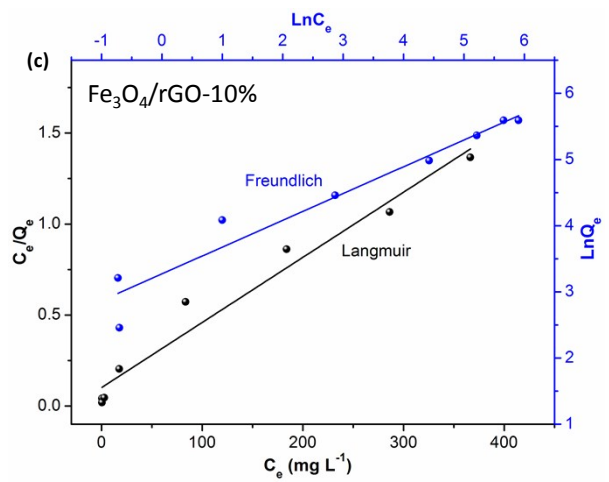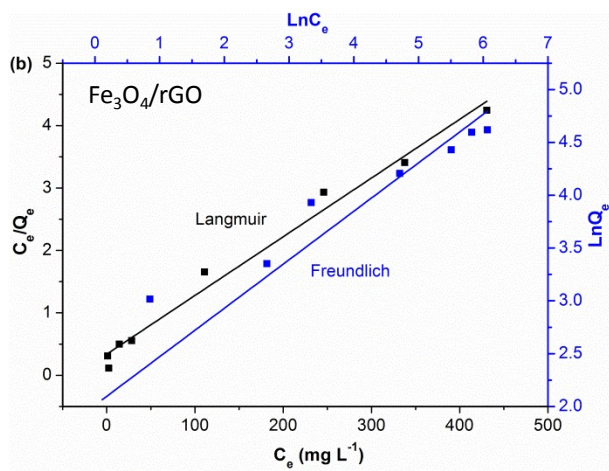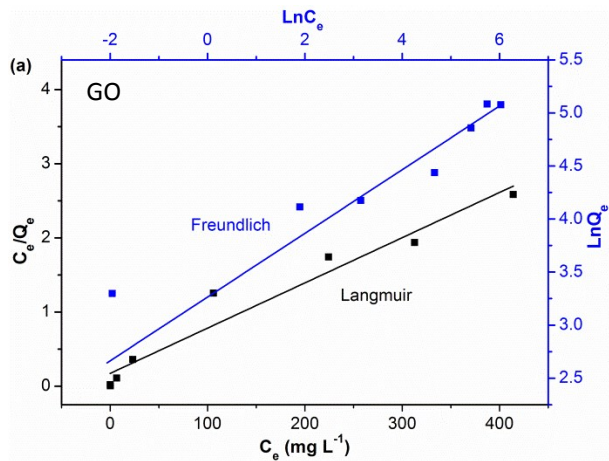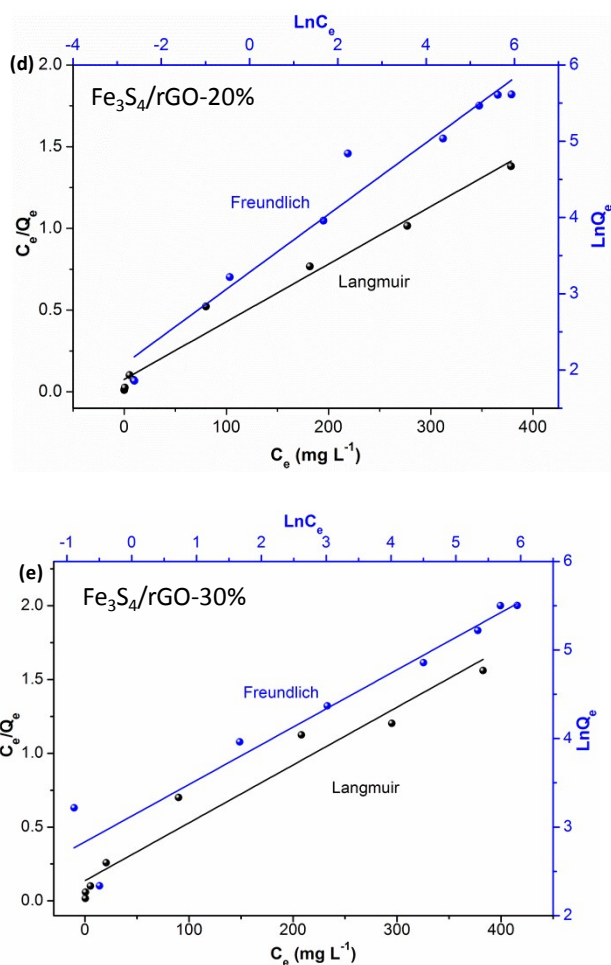
Fig S8 The fittings of Langmuir model and Freundlich model for the adsorption of Pb (II) by GO (a), Fe_3O_4/rGO (b), Fe_3S_4/rGO-10% (c), Fe_3S_4/rGO-20% (d), and Fe_3S_4/rGO-30% (e). The symbols are experimental data; the solid lines represent the fitted curves.
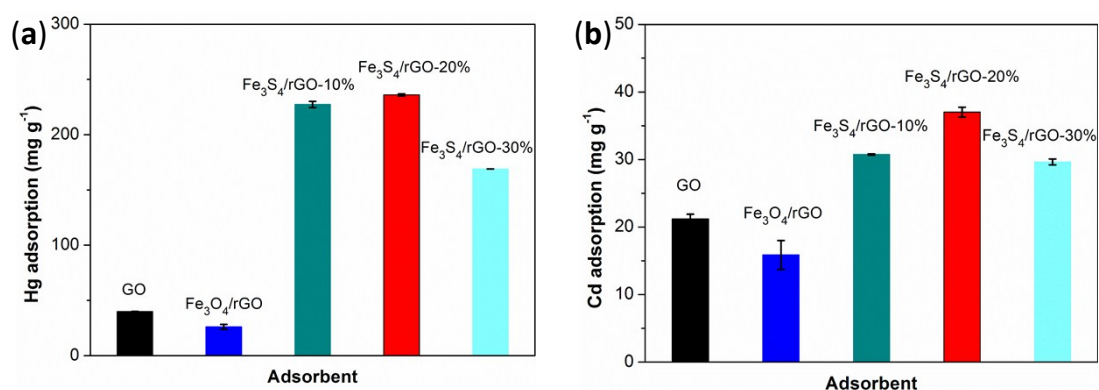
Fig S9 Adsorption performance of GO, Fe_3O_4/rGO, and Fe_3S_4/rGO composites toward (a) Hg (II) and (b) Cd (II). Experimental conditions: initial concentration (60 mg L^{-1} Hg (II), 50 mg L^{-1} Cd (II)) 100 mL, sorbent 25 mg, pH 6, contact time 24 h, temperature 25 °C.
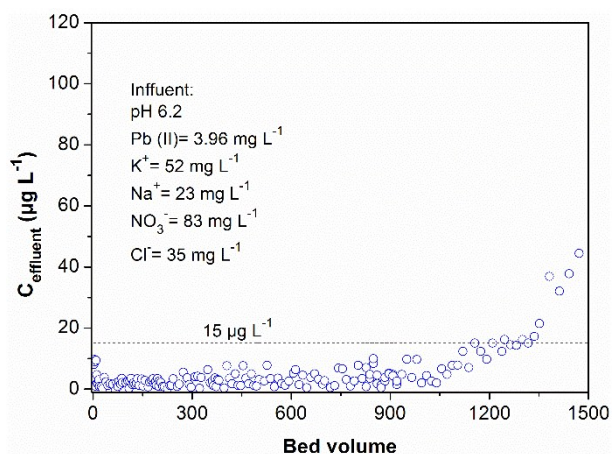
Fig S10 Column adsorption of Pb (II) by Fe_3S_4/rGO from a synthetic Pb (II) feeding solution.
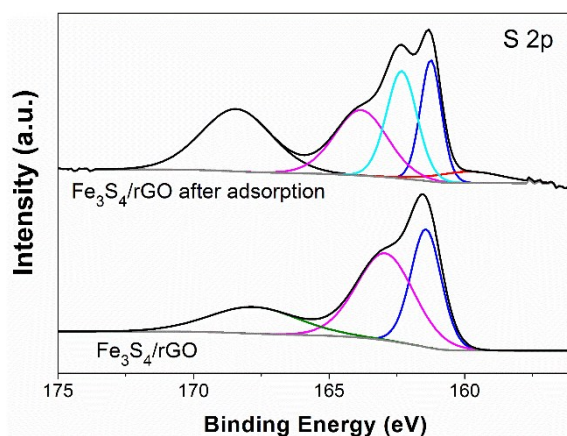
Fig S11 XPS spectra of S 2p for Fe_3S_4/rGO before and after Pb (II) adsorption.

Table S1 Element content of the Fe_3S_4/rGO sample from the XPS analysis.

Name	Pos.	FWHM	Area	At%	Wt%
C 1s	284.82	1.44	10231.13	50.87	29.80
Fe 2p	711.18	4.55	25750.38	12.03	32.76
S 2p	161.33	2.32	5236.89	10.84	10.84
O 1s	531.63	3.19	14818.42	26.26	26.26

Table S2 Contents of the Fe_3O_4/rGO and Fe_3S_4/rGO samples from the TGA analysis.

Sample	Fe_3O_4 (wt%)	Fe_3S_4 (wt%)	rGO (wt%)
Fe_3O_4/rGO-10%	83.25	--	16.75
Fe_3O_4/rGO-20%	75.77	--	24.23
Fe_3O_4/rGO-30%	67.21	--	32.79
Fe_3S_4/rGO-10%	21.36	61.89	16.75
Fe_3S_4/rGO-20%	23.78	51.99	24.23
Fe_3S_4/rGO-30%	19.62	47.59	32.79

Table S3 Adsorption isotherm parameters for Langmuir and Freundlich model of Pb (II) adsorption.

Adsorbent	Langmuir model			Freundlich model		
	Q_m (mg g^{-1})	K_L (L mg^{-1})	R^2	K_F (mg g^{-1})	n	R^2
GO	163.93	0.036	0.984	26.16	3.33	0.849
Fe_3O_4/rGO	106.27	0.028	0.984	7.48	2.18	0.844
Fe_3S_4/rGO-10%	279.33	0.036	0.964	26.36	2.47	0.935
Fe_3S_4/rGO-20%	285.71	0.046	0.976	26.65	2.36	0.950
Fe_3S_4/rGO-30%	255.51	0.029	0.948	22.71	2.48	0.924

Table S4 Comparison of Pb (II) adsorption capacities of various adsorbents

Adsorbent	Sorption capacity (Q_{max} mg g^{-1})	Adsorption conditions	Refs
Graphene nanosheets	35.46	pH 4, 303K	5
Graphene oxide	152.71	pH 4.5, 298K	6
Fe_3O_4	52.94	pH 6, 298K	7
Amorphous Fe_3O_4	22.83	pH = 5 ± 0.2, 303K	8
Porous $NiFe_2O_4$	48.98	pH 5, 308K	9
Fe_2O_3-APTES-EDTA	100.20	room temperature (295-298K).	10
Fe_3O_4-SiO_2-TETA	62.16	pH 7, room temperature	11
multiwall carbon nanotubes/Fe_3O_4 (MWCNTs/ Fe_3O_4)	41.77	pH 5.3, 303K	12
MWCNTs/Fe_3O_4–NH_2	75.02	pH 5.3, 303K	12
Iron oxides	5.60	pH 5.5, 293K	13
MWCNTs/iron oxides	9.85	pH 5.5, 293K	13
MWCNTs/iron oxides/cyclodextrin	12.29	pH 5.5, 293K	13
Thiol-functionalized magnetic mesoporous silica	91.50	pH 6.5, 298K	14
Graphene-Fe_3O_4 composites	69.00	pH 5, 300K	15
Magnetic chitosan/graphene oxide composites	76.94	pH 5, 303K	16
Amino functionalized Fe_3O_4/ graphenes composite	27.95	pH 6-7, room temperature	17
Layered Double Hydroxide Intercalated with MoS_4^{2-} Ions	288.90	pH 5.1, room temperature	18
Fe_3S_4 hollow spheres	92.10	NA	19
Fe_3S_4/rGO-10%	279.33		
Fe_3S_4/rGO-20%	285.71	pH 6, 298K	This work
Fe_3S_4/rGO-30%	255.51		

References:

[1] Ch. Ling, F. Q. Liu, C. Xu, T. P. Chen, A. M. Li, *ACS Appl. Mater. Interfaces*, 2013, **5**, 11808–11817.

[2] Y. H. Li, Q. J. Du, X. D. Wang, P. Zhang, D. C. Wang, Z. H. Wang, Y. Z. Xia, *J. Hazard. Mater*, 2010, **183**, 583–589.

[3] Zhang, Q.; Du, Q.; Hua, M.; Jiao, T.; Gao, F.; Pan, B. *Environ. Sci. Technol.* 2013, **47**, 6536–6544.

[4] Z. S. Wu, S. Yang, Y. Sun, K. Parvez, X. Feng, and K. Müllen, *J. Am. Chem. Soc.*, 2012, **22**, 9082-9085.

[5] Z. H. Huang, X. Zheng, W. Lv, M. Wang, Q. H. Yang, F. Kang, *Langmuir*, 2011, **27**, 7558-7562.

[6] K. Yang, B. Chen, X. Zhu, and B. Xing, *Environ. Sci. Technol.*, 2016, **50**, 11066-11075.

[7] S. Rajput, C. U. Pittman, and D. Mohan, *J. Colloid. Interf. Sci.*, 2016, **468**, 334-346.

[8] C. Zhang, Z. Yu, G. Zeng, B. Huang, H. Dong, J. Huang, Z. Yang, J. Wei, L. Hu, and Q. Zhang, *Chem. Eng. J.*, 2016, **284**, 247-259.

[9] Reddy, D. H. K.; Lee, S.M., *Ind. Eng. Chem. Res.* 2013, **52**, 15789-15800.

[10] Y. Huang, and A. A. Keller, *Water Res*, 2015, **80**, 159-168.

[11] M.E. Mahmoud, M.S. Abdelwahab, and E.M. Fathallah, *Chem. Eng. J.*, 2013, **223**, 318-327.

[12] L. Q. Ji, L. C. Zhou, X. Bai, Y. M. Shao, G. H. Zhao, Y. Z. Qu, C. Wang and Y. F. Li, *J. Mater. Chem.*, 2012, **22**, 15853–15862.

[13] J. Hu, D. D. Shao, C. L. Chen, G. D. Sheng, J. X. Li, X. K. Wang and M. Nagatsu, *J. Phys. Chem. B*, 2010, **114**, 6779–6785.

[14] G. Li, Z. Zhao, J. Liu, G. Jiang, *J. Hazard. Mater.*, 2011, **192**, 277-283.

[15] C. Santhosh, P. Kollu, S. Doshi, M. Sharma, D. Bahadur, M. T. Vanchinathan, P. Saravanan, B. S. Kim, and A. N. Grace, *RSC Adv.*, 2014, **4**, 28300-28308.

[16] L. Fan, C. Luo, M. Sun, X. Li, H. Qiu, *Colloids Surf., B*, 2013, **103**, 523-529.

[17] Guo, X. Y.; Du, B.; Wei, Q.; Yang, J.; Hu, L. H.; Yan, L. G.; Xu, W. Y. *J. Hazard. Mater.* 2014, **278**, 211.

[18] L. Ma, Q. Wang, S. M. Islam, Y. Liu, S. Ma, and M. G. Kanatzidis, *J. Am. Chem. Soc.*, 2016, **138**, 2858-2866.

[19] J. Zheng, Y. Cao, C. Cheng, C. Chen, R. W. Yan, H. X. Huai, Q. F. Dong, M. S. Zheng and C. C. Wang, *J. Mater. Chem. A.,* 2014, **2**, 19882–19888.